Journal of Applied Polymer Science

Microstructure, Rheological Behavior, and Properties of Poly(lactic acid)/Poly(butylene succinate)/Organoclay Nanocomposites

Sophie Risse,[1] Lan Tighzert,[1] Françoise Berzin,[2] Bruno Vergnes[3]
[1]Université de Reims Champagne-Ardenne, LISM EA 4695, 51687, Reims, France
[2]Université de Reims Champagne-Ardenne, INRA, UMR 614 FARE, 51687, Reims, France
[3]MINES ParisTech, CEMEF, UMR CNRS 7635, 06904, Sophia Antipolis, France
Correspondence to: F. Berzin (E-mail: francoise.berzin@univ-reims.fr)

Nanocomposites made of poly(lactic acid), poly(butylene succinate), and organically modified montmorillonite were prepared by melt blending in a twin screw extruder. The influence of the organoclay content on nanocomposite properties was investigated. The nanocomposite structure has been characterized by various techniques at different scales. X-ray diffraction showed an intercalated structure whereas rheological investigations in small amplitude oscillatory shear indicated a partial exfoliation. It was also shown that organoclay was evenly dispersed in the matrix even though some large aggregates were also observed. The mechanical properties of nanocomposites were measured in uniaxial tensile test. Oxygen and water vapor permeability was also characterized. It was shown that dispersed organoclay and aggregates have a direct impact on mechanical properties and permeability. An increase of Young's modulus by 41% and a decrease of permeability by 40% could be obtained with 7 wt % organoclay. © 2014 Wiley Periodicals, Inc. J. Appl. Polym. Sci. **2014**, *131*, 40364.

KEYWORDS: nanocomposites; mechanical properties; polyesters; rheology; structure-property relations

Received 26 September 2013; accepted 27 December 2013
DOI: 10.1002/app.40364

INTRODUCTION

Polymer blending is an interesting way to obtain new materials with combined properties of each polymer.[1] Main polymers are immiscible, leading to heterogeneous morphologies. It is well known that the morphology has a direct impact on blend properties. For example, a fibrillar morphology improves tensile properties, a droplet/matrix configuration results in better impact properties, a lamellar morphology induces barrier properties and a co-continuous morphology presents a combination of the characteristics of both polymers. The last two morphologies lead usually to interesting properties for conductivity or permeability.[2,3] Poly(lactic acid) (PLA) and poly(butylene succinate) (PBS) are two interesting polymers for blending because of their complementary mechanical properties: PLA is rigid and brittle while PBS is soft and ductile. Further, both polymers are biodegradable and their permeability to water vapor is relatively high compared to that of polyethylene (PE), while their permeability to oxygen is markedly lower. PLA/PBS blends have attracted much attention in recent years.[4–9] However, the low water vapor barrier properties are one of the major drawbacks of these polyesters and limit their development for packaging applications when high barrier properties are required.

Incorporating nanoclay in a polymer matrix is one of the most promising techniques for decreasing the matrix permeability. Usually, a decrease in oxygen or water vapor permeability in blends is due to an increase in tortuosity due to the presence of nanoparticles, which increases the distance that permeating molecule has to overcome through the sample.[10–12] The direct melt intercalation is one of the most common techniques for preparing polymer/organoclay nanocomposites. The dispersion of organoclay in polymer matrix is greatly dependent on the extrusion parameters like feed rate, screw profile, and screw speed.[13–15] The clay is generally functionalized by quaternary ammonium surfactants to enhance the affinity between hydrophobic matrix and hydrophilic clay. It is well known that, in the case of polymer blends, the organoclay play a role of compatibilizer, decreasing the size of the dispersed phase.[16–18] The role of the surfactant in this compatibilizing effect was recently demonstrated for PET/PE blends.[19] The final properties of the nanocomposites depend on the microstructure and the organoclay level of dispersion. Hence, it is important to characterize the dispersion of organoclay in polymer matrix, at different levels. X-ray diffraction (XRD) can be easily used to quantify the intercalation of polymer matrix in the silicate layers. Transmission electron microscopy (TEM) observations coupled with

rheological investigations allow quantifying the exfoliation. Scanning electron microscopy (SEM) can be used to observe the microscopic structure and eventually the presence of aggregated particles.

The objective of this study is to examine the influence of the blend morphology and the dispersion of organoclay on the mechanical properties and the permeability of PLA/PBS blends, prepared by melt mixing in a twin screw extruder, using different clay contents.

EXPERIMENTAL

Materials

The two polymers used in this study were commercially available PLA and PBS. The organically modified montmorillonite (OMMT) used was the Cloisite©30B (Cl30B) provided by Southern Clay Products. It is a pristine MMT modified with 30 wt % of methyl tallow bis(2-hydroxyethyl) quaternary ammonium chloride. Tallow (T) is composed of around 65% C18, 30% C16, and 5% C14.

Samples Preparation

The pellets of both polymers and the organoclay were dried in a vacuum oven overnight at 60°C and 80°C, respectively. Cl30B was incorporated at 3, 4.5, and 7 wt % into the blends of PLA/PBS (50/50 wt %). Nanocomposites with 3, 4.5, and 7 wt % of Cl30B will be subsequently named PLA/PBS/Cl30B 3%, PLA/PBS/Cl30B 4.5%, and PLA/PBS/Cl30B 7%. The nanocomposites were prepared using a laboratory scale twin screw extruder Clextral BC 21 (Firminy, France). It has a diameter D of 25 mm and a length L of 900 mm (L/D ratio: 36). All blends were prepared under the same extrusion conditions: the screw speed was set-up at 250 rpm, the feed rate at 6 kg h^{-1}, and the barrel temperatures between 60°C for barrel 1 and 160°C for barrel 9. For each sample, extruded strings were collected at the die exit and rapidly cooled in water for subsequent analyses.

Characterization

The morphology of the blends was examined on cryogenically fractured samples by field emission gun-SEM (FEG-SEM) (Zeiss Supra 40) with an accelerating voltage between 3 and 15 kV. Prior to the observation, the samples surface was coated by platinum (around 10 nm).

Wide angle X-ray diffraction (WAXD) experiments were performed using a Bruker D8 Advance diffractometer, with Cu-$K\alpha$ radiation of wavelength 1.54 Å. The accelerating voltage was 40 kV. Diffraction data were obtained over a 2θ range of 2°–10° and the interlayer spacing d_{001} was calculated using the Bragg's equation.

Rheological measurements in small amplitude oscillatory shear (SAOS) were performed on a parallel-plate rheometer (AR2000ex, TA Instruments), with a diameter of 25 mm and a gap of 1 mm. Test specimens were prepared by compression molding at 180°C. Storage and loss modulus were measured over a frequency range of 100–0.1 rad s^{-1} at different temperatures: 170°C, 180°C, 190°C, and 200°C. Before the frequency sweep, a strain sweep was performed (at a temperature of 190°C and a frequency of 1 rad s^{-1}) to ensure that the strain used was within the linear viscoelastic range.

Tensile tests were carried out at room temperature using a tensile machine (MTS Adamel Lhomargy-DY35XL) at a crosshead speed of 10 mm min^{-1} on samples prepared by injection. A 20 kN load cell was used. A minimum of ten specimens was tested and the average value was reported.

Oxygen permeabilitiy of nanocomposite films was measured using a Mocon Oxtran® 2/21. The Oxtran technology is based on a flow system in which oxygen passes on one side of the film mounted in a diffusion cell while an inert carrier gas flows on the other side. The carrier gas sweeps oxygen to a coulometric detector. Pure oxygen was used as test gas and pure nitrogen as carrier gas. Testing was performed at 23°C and 50% relative humidity (RH) (on both sides of the specimen). The gradient in partial pressure of oxygen was 1 bar. The values will be thus expressed in mL mm (m^2 day^{-1}) which are the same in mL mm/(m^{-2} $day^{-1}bar^{-1}$).

Water vapor permeability was measured on nanocomposite films using a Mocon Permatran W® 3/33. The principle of the Permatran technology is globally the same, only the test gas is different. In this method, a dry chamber is separated by the specimen from a wet chamber of known temperature and humidity. Testing was also performed at 23°C and 50% RH. The RH of the test gas was thus 50% and the carrier gas was dry pure nitrogen. The detector was an infrared detector. For each blend, the value reported is the average of two measurements.

RESULTS AND DISCUSSION

Cl30B is initially in the form of agglomerates of a few tenths of microns. One of the main objectives of the compounding process is to destroy these agglomerates and to disperse the tactoids in order to reach a maximum of exfoliation. With the selected formulation (50/50), the blend morphology is expected to be co-continuous, but the location of the organoclay (in PLA, in PBS, at the interface) remains open.

X-ray Diffraction

The intercalation state of Cl30B in the PLA/PBS blends was examined using WAXD measurements. The WAXD patterns of native Cl30B and nanocomposites are shown in Figure 1. The peak at 4.83° corresponds to the interlayer spacing of Cl30B, equal to 1.82 nm. For all nanocomposites, the characteristic peaks of basal distance d_{001} were strongly shifted to lower angles, indicating an intercalated structure. The interlayer spacing d_{001} was around 3.17 nm, almost constant for all nanocomposites. The amount of Cl30B seems to have no significant influence on the state of intercalation. The absence of the basal reflection of the native clay could indicate that the structure is fully intercalated for all nanocomposites. However, a second weak peak is observed at a higher angle, corresponding to an interlayer spacing of around 1.57 nm, which is probably due to the second order reflection.[20,21]

FEG-SEM Observations

Figure 2 shows FEG-SEM micrographs of the fracture surface of PLA/PBS/Cl30B blends. Their morphology varies with the

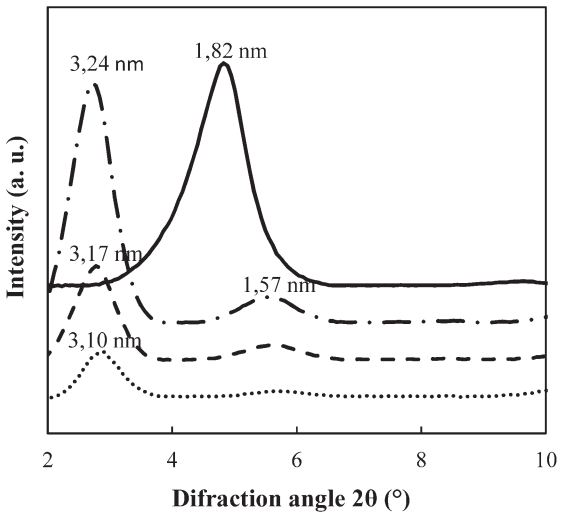

Figure 1. WAXD patterns of organoclay Cl30B (*black full line*), PLA/PBS matrix (*gray full line*), and PLA/PBS/Cl30B nanocomposites (··· PLA/PBS/Cl30B 3%, – – – PLA/PBS/Cl30B 4.5%, and – · – PLA/PBS/Cl30B 7%).

Cl30B content. Effectively, with 3 wt % of Cl30B [Figure 2(a)], the two phases seem to form a co-continuous morphology. Some fine filaments are visible, probably due to the PBS deformation during the cryogenic fracture. When the clay content increases to 4.5 wt %, the co-continuous morphology becomes more laminar [Figure 2(b)]. However, with 7 wt % of Cl30B [Figure 2(c)], the morphology becomes finer and even more layered, as composed by a superposition of very thin sheets.

No aggregates are visible at this scale on these three micrographs, but some other pictures show aggregates with a diameter of around a tenth of microns for 3 wt % and around one hundred of microns for the other contents. Figure 3 is an example of large aggregate present in the blend with 4.5 wt % of Cl30B. An energy dispersive spectrometry (EDS) analysis confirmed that these aggregates are effectively made of organoclay not dispersed into the matrix. EDS analyses were also performed on different locations and showed that clay is evenly dispersed into the matrix, even though it is not visible on the FEG-SEM micrographs. Apparently, there is no particular location of the clay, which seems to be present everywhere in the matrix.

Rheological Behavior

Figure 4 shows the storage modulus G' of the matrix and the different nanocomposites as function of strain amplitude. Similar trends were observed for the loss modulus (not shown here). The PLA/PBS blend without Cl30B displays a linear viscoelastic behavior for strains up to about 20%. For the PLA/PBS/Cl30B blends, the end of linear viscoelastic behavior occurs at lower strain values. This critical strain γ_c decreases with the percentage of Cl30B, from 0.50% to 0.35% and 0.25% for 3%, 4.5%, and 7% of organoclay, respectively. This is typical of the Payne effect and well known for filled polymers.[22,23] Moreover, the value of the storage modulus in the linear viscoelastic region G'_0 increases with the Cl30B content. The organoclay has clearly a reinforcing effect on the polymer matrix.

The normalized storage modulus G'/G'_0 is plotted as a function of normalized strain γ/γ_c in Figure 5 for PLA/PBS/Cl30B nanocomposites. This mastercurve describes the global behavior during the transition between linear and non-linear region and confirms the values of G'_0 and γ_c measured previously. Moreover, it can be shown that the critical strain γ_c scales with the clay volume fraction ϕ as $\gamma_c \propto \phi^{-\nu}$ where ν is equal to 0.8, what is close to the values generally found for clay nanocomposites.[21,23]

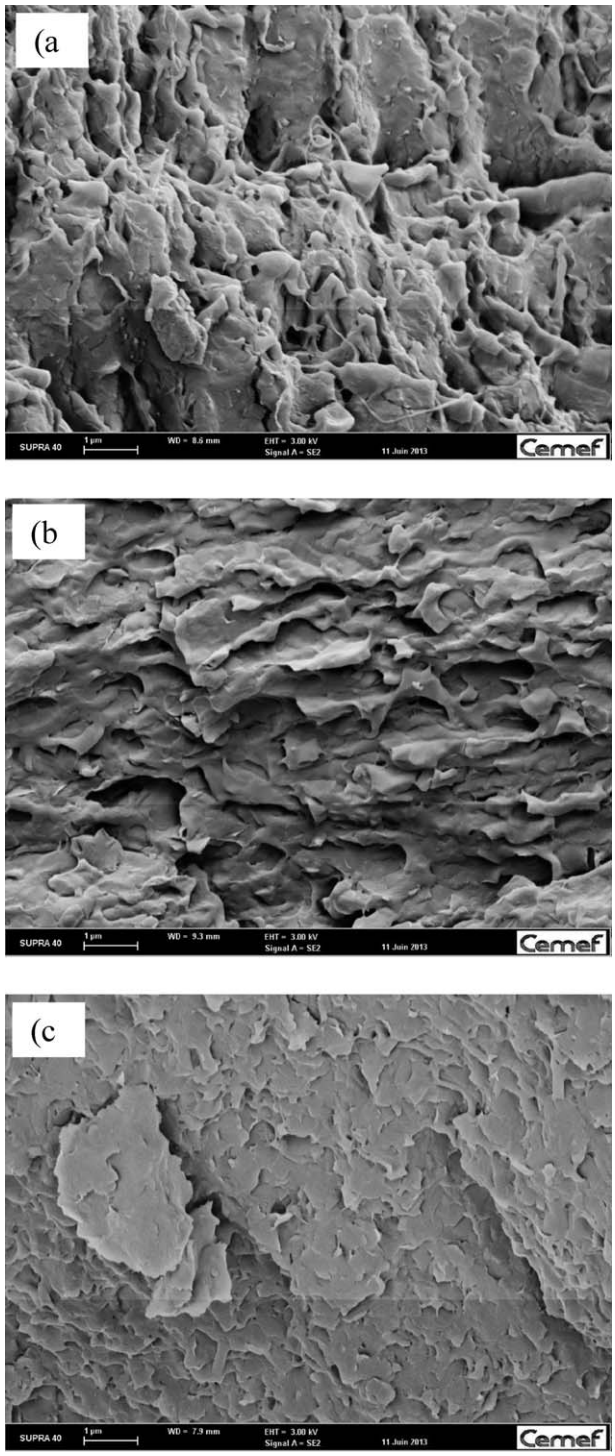

Figure 2. FEG-SEM micrographs of three nanocomposites: PLA/PBS/Cl30B 3% (**a**), PLA/PBS/Cl30B 4.5% (**b**), and PLA/PBS/Cl30B 7% (**c**).

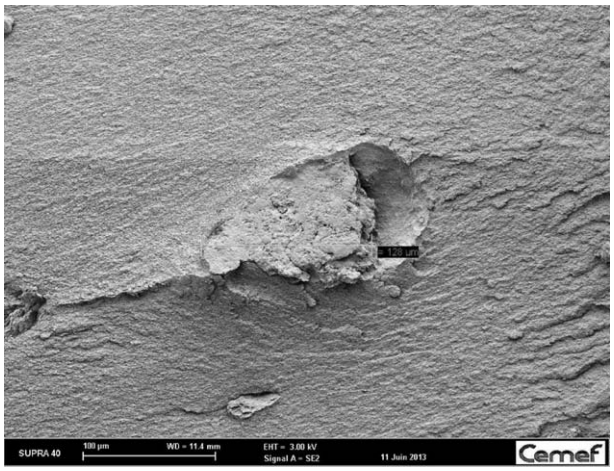

Figure 3. FEG-SEM picture of a Cl30B aggregate in the PLA/PBS/Cl30B 4.5% nanocomposite.

The storage and loss modulus of the various materials were measured at four temperatures, from 170°C to 200°C. Figure 6 shows the values of G' at 180°C. First, it can be noticed that, for PLA/PBS matrix in the terminal region, the slope of log G' versus log ω is <2 (value of 0.94). Similarly, the slope of log G'' versus log ω (not shown here) is also <1 (value of 0.83). This result may be explained by the polydispersity of the PBS.[24] Indeed this commercial polymer has a different behavior from that observed for classical monodispersed polymers. The slopes of log G' versus log ω in the terminal region for neat PLA and PBS are equal to 1.9 and 0.8 for neat PLA and neat PBS, respectively.

The behavior of the blends with Cl30B can now be discussed. A plateau of the storage modulus is observed for these materials at low frequency. Its origin is due to the existence of a three-dimensional percolated network structure.[25–28] Moreover, the G' value at plateau increases with Cl30B amount, as already seen in Figure 4.

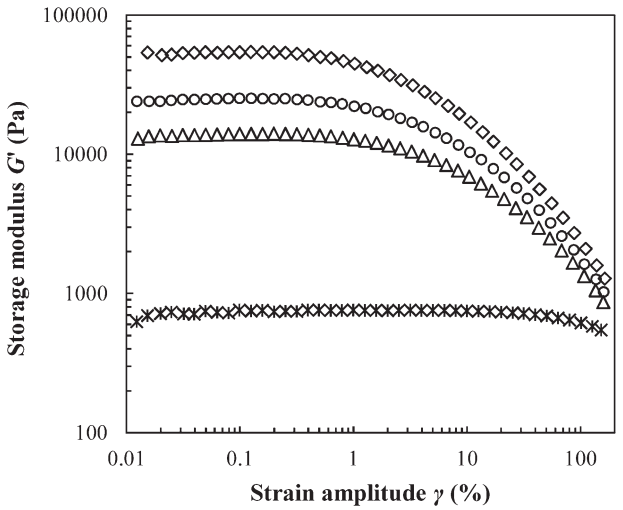

Figure 4. Strain dependence of neat PLA/PBS and PLA/PBS/Cl30B nanocomposites at 190°C and $\omega = 1$ rad s^{-1} (* PLA/PBS, △ PLA/PBS/Cl30B 3%, ○ PLA/PBS/Cl30B 4.5%, ◇ PLA/PBS/Cl30B 7%).

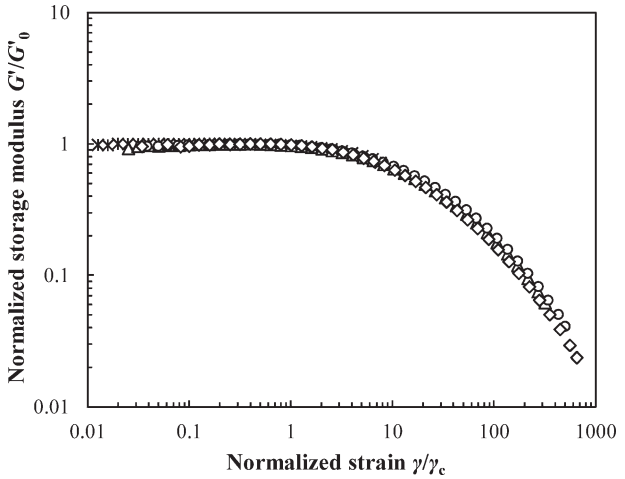

Figure 5. Mastercurve of normalized storage modulus G'/G'_0 as function of normalized strain γ/γ_c at 180°C (* PLA/PBS, Δ PLA/PBS/Cl30B 3%, ○ PLA/PBS/Cl30B 4.5%, ◇ PLA/PBS/Cl30B 7%).

Figure 7 presents the complex viscosity $|\eta^*|$ as function of frequency for the various blends. The viscosity curves are presented after time–temperature superposition (TTS) at the reference temperature of 180°C. Even though it has been recently reported that TTS principle fails for some nanocomposites due to time evolution of the nanostructure,[28] in the present case it applied nicely. It means that the same nanostructure was probed at the different temperatures and that this structure did not change a lot with time in the range of temperature studied.

In the low frequency range, the blend without Cl30B exhibited a Newtonian behavior and the whole viscosity curve can be fitted by a Carreau–Yasuda law. However, with Cl30B, an increase in complex viscosity is observed, related to the development of the storage modulus plateau seen in Figure 6. The complex viscosity of the nanocomposites can now be described by the Carreau–Yasuda law with a yield stress:[29,30]

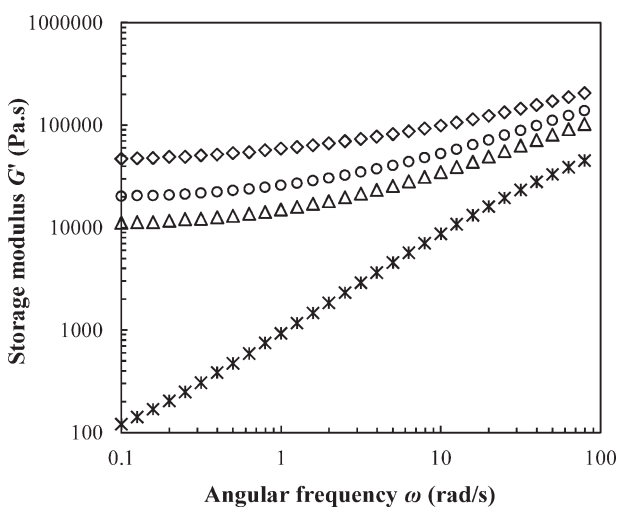

Figure 6. Comparison of the storage modulus G' of neat PLA/PBS and PLA/PBS/Cl30B nanocomposites at 180°C (* PLA/PBS, △ PLA/PBS/Cl30B 3%, ○ PLA/PBS/Cl30B 4.5%, ◇ PLA/PBS/Cl30B 7%).

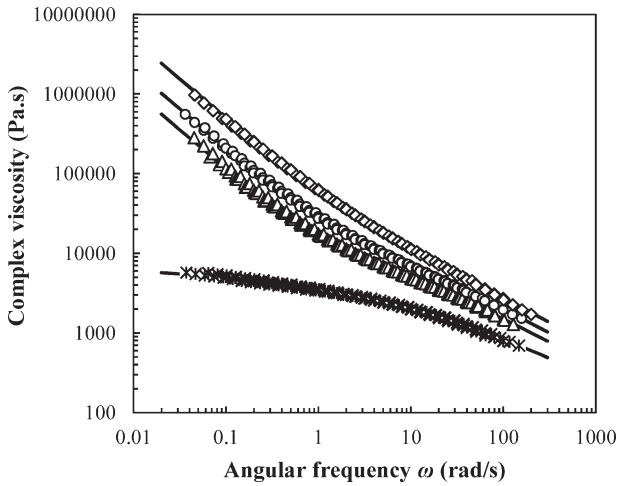

Figure 7. Comparison of the complex viscosity of neat PLA/PBS and PLA/PBS/Cl30B nanocomposites at 180°C (* PLA/PBS, Δ PLA/PBS/Cl30B 3%, ○ PLA/PBS/Cl30B 4.5%, ◇ PLA/PBS/Cl30B 7%). Symbols are experimental data, solid lines are fits with eq. (1).

$$|\eta^*(\omega)| = \frac{\sigma_0}{\omega} + \eta_0[1+(\lambda\omega)^a]^{\frac{m-1}{a}} \quad (1)$$

where σ_0 is the melt yield stress, η_0 the Newtonian viscosity, λ is the time constant, m the dimensionless power law index, and a is the Yasuda parameter. The five parameters were first determined for the blend without Cl30B (in this case, $\sigma_0 = 0$). The obtained values were then used as starting parameters for the blends with Cl30B. The slopes of complex viscosity curves at high frequencies are the same for all PLA/PBS/Cl30B blends. Hence, the power law index could be assumed equal to 0.53 for all blends which is the value found for the PLA/PBS matrix.

Figure 7 shows the superposition between the experimental data and the fitted curves of $|\eta^*|$. The corresponding data is given in Table I. In all cases, the superposition between experimental data and the fitted curves is very satisfactory. Figure 8 shows the evolution of some parameters of the Carreau–Yasuda law. The evolution of the zero shear viscosity η_0 with clay content is essentially due to hydrodynamic effects. Accordingly, we can fit this evolution with a typical law for suspensions,[31,32] like for example:

$$\eta = \eta_0\left(1-\frac{\varphi}{\varphi_{max}}\right)^{-\alpha} \quad (2)$$

where η_0 is the viscosity of the suspending fluid (here, the PLA/PBS blend), η the viscosity of the suspension at a volume fraction φ, φ_{max} the maximum volume fraction and α a constant. On Figure 8(a), we can see that we obtain a correct fit with $\varphi_{max} = 10.5\%$ and $\alpha = 2.2$, which is very close to the usual value of 2.

Table I. Parameters of the Carreau–Yasuda Law with Yield Stress

Cl30B content (wt %)	0	3	4.5	7
σ_0 (Pa)	0	10,586	19,461	45,307
η_0 (Pa s)	6202	10,750	14,100	19,850
λ (s)	0.47	0.62	0.72	1.00
m	0.53	0.53	0.53	0.53
a	0.45	0.65	0.74	1.74

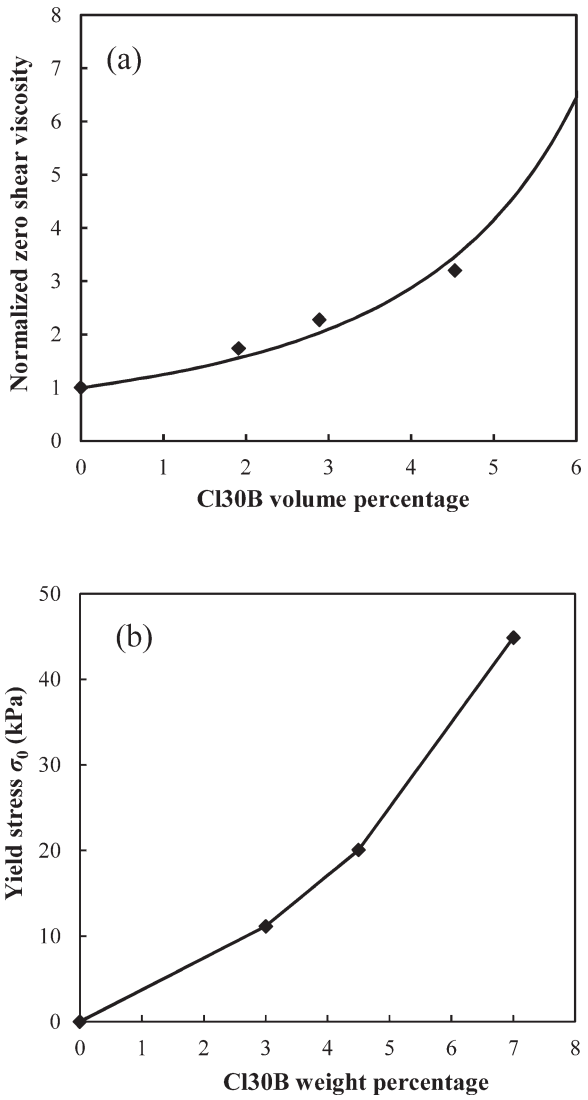

Figure 8. Evolution of normalized Newtonian viscosity (**a**) and melt yield stress σ_0 (**b**) with Cl30B content for the PLA/PBS/CL30B nanocomposites.

Figure 8(b) shows that the melt yield stress strongly increases with the Cl30B content. It is explained by the increase of interactions between the clay tactoïdes and platelets, due to both increase of clay content and possibly improvement in the level of exfoliation.[29] In order to try to separate the effects of clay content and level of exfoliation, we may assume that the behavior at high frequency is dictated by hydrodynamic effects, described by eq. (2). If we normalize the complex viscosity by the zero shear viscosity η_0, for the same level of exfoliation, we would obtain a mastercurve. We can see in Figure 9 that it is not the case: if the curves are superimposed at high frequency, they diverge rapidly, indicating strong interactions between the exfoliated platelets. Moreover, they are different for the various clay contents, what means the exfoliation level increases between

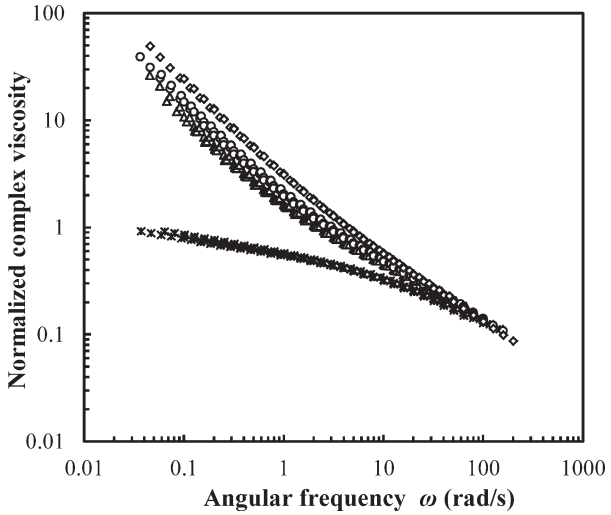

Figure 9. Comparison of the normalized complex viscosity of neat PLA/PBS and PLA/PBS/Cl30B nanocomposites at 180°C (* PLA/PBS, Δ PLA/PBS/Cl30B 3%, ○ PLA/PBS/Cl30B 4.5%, ◇ PLA/PBS/Cl30B 7%).

3 and 7 wt %. On the normalized curves, the level of exfoliation is now related to the ratio σ_0/η_0. This parameter is equal to 0.98, 1.38, and 2.28 for 3 wt %, 4.5 wt %, and 7 wt %, respectively. Consequently, we can conclude that the level of clay exfoliation increases with the clay content.

Mechanical Properties

As explained before, the structure of the various nanocomposites is intercalated and partially exfoliated, with higher exfoliation at higher clay content. Figure 10 presents the evolution of the Young's modulus and the elongation at break of PLA/PBS/Cl30B blends as function of the organoclay content. The Young's modulus increases continuously with the clay content. An improvement of about 15% is observed with an addition of 4.5 wt % of Cl30B, whereas a maximum of 41% improvement is noted with an addition of 7 wt %. A lot of studies have shown an increase in Young's modulus with nanoclay for other polymer matrices like polypropylene,[33] polyamide 6,[34,35] polyimide,[36] or epoxy resins.[37] The elongation at break remains

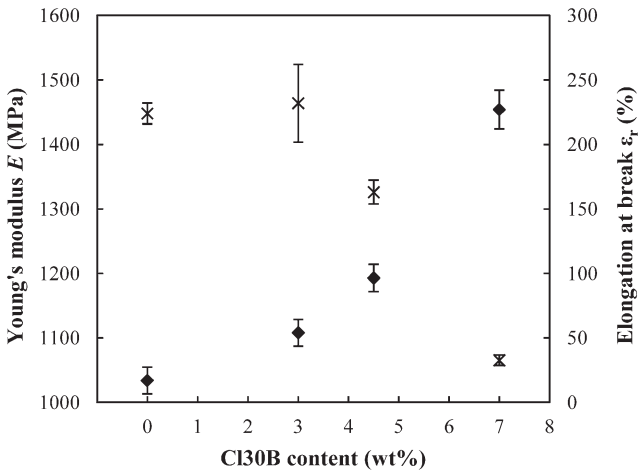

Figure 10. Young's modulus (◆) and elongation at break (×) as function of Cl30B content.

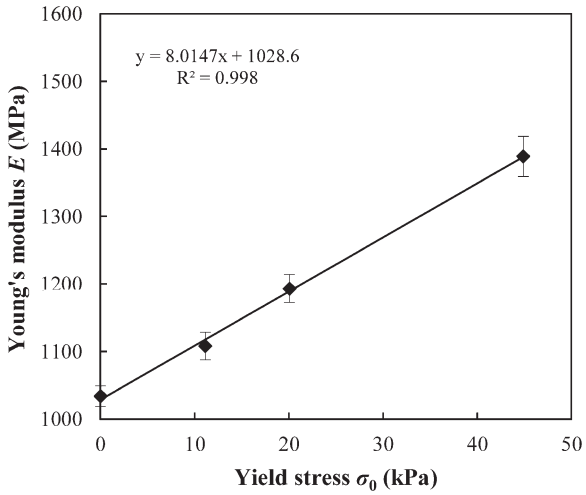

Figure 11. Young's modulus as function of melt yield stress.

almost constant up to about 3 wt % of Cl30B and then falls rapidly. The nanocomposite with 7 wt % of Cl30B is brittle, with a 85% decrease in elongation at break compared to the pure matrix. The elongation at break is probably reduced because of the presence of large clay aggregates in the blends, which can potentially induce crack initiation.[34,35]

In Figure 11 the Young's modulus of nanocomposites is plotted as a function of the yield stress. It increases linearly, indicating an improved reinforcement with both the clay content and the level of exfoliation.

Oxygen and Water Vapor Permeability

The permeability coefficients obtained for oxygen and water vapor at 23°C and 50% RH are reported in Figure 12. Both permeabilities diminish with the addition of Cl30B. Organoclays enhance the gas barrier properties by creating a tortuous path that retards or even prevents the progress of gas molecules through the polymer matrix.[10–12] The value of permeability of PLA/PBS blend is reduced by 40% for O_2 and by 50% for the water vapor with 7 wt % of clay. Surprisingly, in the range investigated, the evolution is perfectly linear for both oxygen and water vapor. As shown before, the morphology of the nanocomposite is partially intercalated and exfoliated, with residual clay aggregates. It is difficult to quantify the real influence of aggregates on permeability. However, we believe that permeability could be reduced even more if these aggregates were fully exfoliated. Indeed, according to the Nielsen model, the relative permeability coefficient depends on the volume fraction of the dispersed clay particles and on the platelets dimensions.[38] Clay aggregates could have damaging effect on barrier properties. Concerning the linear evolution with the clay content, studies on PLA oxygen permeability with various fillers (OMSFM, organically modified synthetic fluorine mica,[39] Cloisite 25A,[40] another OMMT of Southern Clays Products) rather showed a convex evolution. Ray et al.[39] showed that the major part of OMSFM layers in PLA/OMSFM nanocomposites were exfoliated and that the intercalated layers had only a very small effect on O_2 gas barrier properties. It can thus be supposed that intercalated Cl30B layers do not change the permeability, but

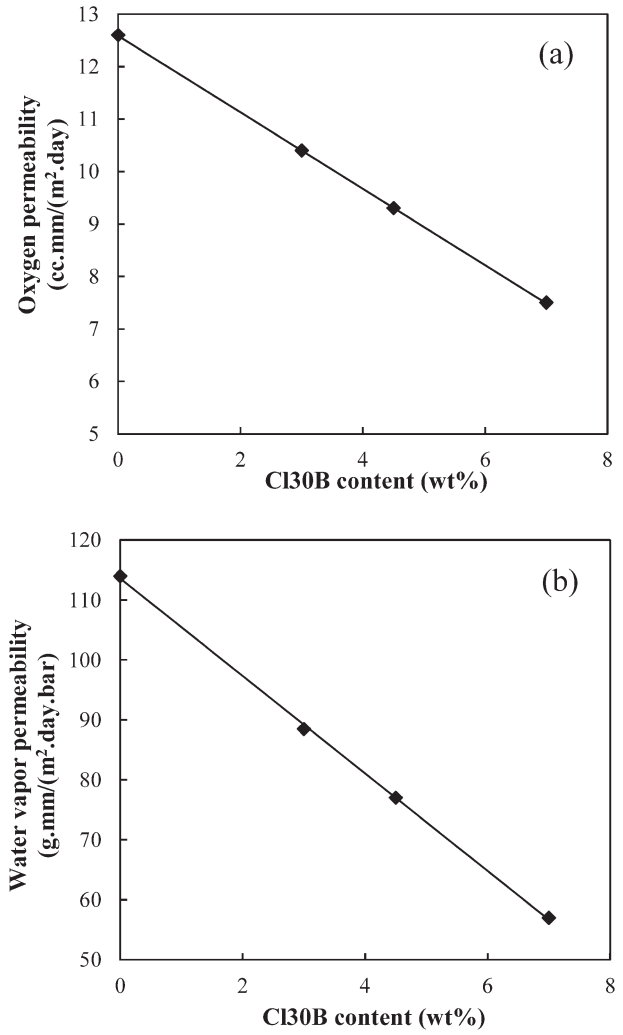

Figure 12. Oxygen permeability (**a**) and water vapor permeability (**b**) of neat PLA/PBS and PLA/PBS/Cl30B nanocomposites as function of Cl30B content at 23°C and 50% RH.

that the aggregates strongly raise it. Consequently, the obtained linear diminution of O_2 and water vapor permeability is not the maximal reduction of permeability for the different PLA/PBS/Cl30B nanocomposites. A change in the processing conditions could probably allow to improve the exfoliation and thus to reduce even more the permeability.[13,15,33]

CONCLUSIONS

In this study, we have characterized the properties of nanocomposites based on blends of PLA, PBS, and organoclay. Blends with the same formulation (50/50 wt %) but different clay contents have been prepared in fixed processing conditions, by melt mixing in a twin screw extruder. First of all, the morphology of the blends is strongly affected by the clay content, varying from co-continuous to lamellar. It has been proved by EDS analysis that the clay was evenly dispersed into the matrix. SEM-FEG observations showed the presence of residual large clay aggregates. XRD allowed to determine an intercalated structure for all nanocomposites, whereas rheological investigations indicated a partial exfoliation, related to the value of the melt yield stress. The exfoliation level was shown to increase with clay content. Young's modulus increased and deformation at break decreased when increasing clay content. At low contents of Cl30B and without clay aggregates, the PLA/PBS/Cl30B blends show a ductile behavior. With a Cl30B ratio equal or superior to 7 wt %, they become brittle due to incomplete dispersion of organoclay. Further, the incorporation of Cl30B enhances barrier properties of PLA/PBS blends, but the presence of aggregates is harmful to the impermeability of gas, such like oxygen and water vapor. Studies are going on to improve the clay dispersion, consequently to increase mechanical and barrier properties.

ACKNOWLEDGMENTS

The authors are indebted to Gaïa Biopackaging (Brive La Gaillarde, France) for financial support, Nathalie Choiselle, Philippe Dony (Université de Reims Champagne-Ardenne), and Suzanne Jacomet (CEMEF, MINES ParisTech) for helpful technical assistance.

REFERENCES

1. Utracki, L.A. Polymer Blends Handbook, Kluwer, **2002**.
2. Willemse, R. C.; Posthuma de Boer, A.; Van Dam, J.; Gotsis, A. D. *Polymer* **1998**, *39*, 5879.
3. Chaput, S.; Carrot, C.; Castro, M.; Prochazka, F. *Rheol. Acta* **2004**, *43*, 417.
4. Park, J. W.; Im, S. S. *J. Appl. Polym. Sci.* **2002**, *86*, 647.
5. Bhatia, A.; Gupta, R.; Bhattacharya, S.; Choi, H. *Korea-Aust. Rheol. J.* **2007**, *19*, 125.
6. Yokohara, T.; Yamaguchi, M. *Eur. Polym. J.* **2008**, *44*, 677.
7. Bhatia, A.; Gupta, R. K.; Bhattacharya, S. N.; Choi, H. J. *J. Appl. Polym. Sci.* **2009**, *114*, 2837.
8. Chen, G. X.; Kim, H. S.; Kim, E. S.; Yoon, J. S. *Polymer* **2005**, *46*, 11829.
9. Wu, D.; Yuan, L.; Laredo, E.; Zhang, M.; Zhou, W. *Ind. Eng. Chem. Res.* **2012**, *51*, 2290.
10. Sinha Ray, S.; Okamoto, M. *Prog. Polym. Sci.* **2003**, *28*, 1539.
11. Bharadwaj, R. K. *Macromolecules* **2001**, *34*, 9189.
12. Sinha Ray, S.; Yamada, K.; Okamoto, M.; Fujimoto Y.; Ogami, A.; Ueda, K. *Polymer* **2003**, *44*, 6633.
13. Lertwimolnun, W.; Vergnes, B. *Polym. Eng. Sci.* **2007**, *47*, 2100.
14. Dennis, H.; Hunter, D.; Chang, D.; Kim, S.; White, J.; Cho, J.; Paul, D. *Polymer* **2001**, *42*, 9513.
15. Domenech, T.; Peuvrel-Disdier, E.; Vergnes, B. *Compos. Sci. Technol.* **2013**, *75*, 7.
16. Sinha Ray, S.; Pouliot, S.; Bousmina, M.; Utracki, L. A. *Polymer* **2004**, *45*, 8403.
17. Sinha Ray, S.; Bousmina, M. *Macromol. Rapid Commun.* **2005**, *26*, 450.
18. Sinha Ray, S.; Bousmina, M. *Macromol. Rapid Commun.* **2005**, *26*, 1639.
19. Yousfi, M.; Soulestin, J.; Vergnes, B.; Lacrampe, M. F.; Krawczak, P. *J. Appl. Polym. Sci.* **2013**, *128*, 2766.

20. Giannelis, E. P.; Krishnamoorti, R.; Manias, E. In Polymers in Confined Environments; Advances in Polymer Science; Springer: Berlin Heidelberg, **1999**; Vol. *138*, pp 107–147.
21. Ghanbari, A.; Heuzey, M. C.; Carreau, P. J.; Ton-That, M. T. *Rheol. Acta* **2013**, *52*, 59.
22. Payne A. R. Reinforcement of Elastomers; Interscience: New York, **1965**; pp 69–123.
23. Cassagnau P. *Polymer* **2008**, *49*, 2183.
24. Han, C. D. Rheology and Processing of Polymeric Materials. Volume 1: Polymer Rheology; Oxford University Press: New York, **2007**.
25. Galgali, G.; Ramesh, C.; Lele, A. *Macromolecules* **2001**, *34*, 852.
26. Solomon, M. J.; Almusallam, A. S.; Seefeldt, K. F.; Somwangthanaroj, A.; Varadan, P. *Macromolecules* **2001**, *34*, 1864.
27. Ren, J.; Silva, A. S.; Krishnamoorti, R. *Macromolecules* **2000**, *33*, 3739.
28. Zouari, R.; Domenech, T.; Vergnes, B.; Peuvrel-Disdier, E. *J. Rheol.* **2012**, *56*, 725.
29. Vergnes, B. *Int. Polym. Process.* **2011**, *26*, 229.
30. Lertwimolnun, W.; Vergnes, B. *Polymer* **2005**, *46*, 3462.
31. Krieger, I. M.; Dougherty, T. *J. Trans. Soc. Rheol.* **1959**, *3*, 137.
32. Mewis, J.; Wagner, N. J. *J. Non-Newt. Fluid Mech.* **2009**, *157*, 147.
33. Domenech, T.; Peuvrel-Disdier, E.; Vergnes B. *Int. Polym. Process.* **2012**, *27*, 517.
34. Fornes, T. D.; Yoon, P. J.; Keskkula, H.; Paul, D. R. *Polymer* **2001**, *42*, 9929.
35. Masenelli-Varlot, K.; Reynaud, E.; Vigier, G.; Varlet, J. *J. Polym. Sci. Part B Polym. Phys.* **2002**, *40*, 272.
36. Agag, T.; Koga, T.; Takeichi, T. *Polymer* **2001**, *42*, 3399.
37. Yasmin, A.; Abot, J. L.; Daniel, I. M. *Scr. Mater.* **2003**, *49*, 81.
38. Nielsen, L. E. *J. Macromol. Sci. Part A - Chem.* **1967**, *1*, 929.
39. Sinha Ray, S.; Yamada, K.; Okamoto, M.; Ogami, A.; Ueda, K. *Chem. Mater.* **2003**, *15*, 1456.
40. Chang, J. H.; An, Y. U.; Sur, G. S. *J. Polym. Sci. Part B Polym. Phys.* **2003**, *41*, 94.